

## Local boundary-layer receptivity to a convected free-stream disturbance

By A. J. DIETZ

Fluid Mechanics Laboratory, NASA Ames Research Center, Moffett Field, CA 94035, USA

(Received 12 February 1998 and in revised form 6 August 1998)

An investigation of the local receptivity of a Blasius boundary layer to a harmonic vortical disturbance is presented as a step towards understanding boundary-layer receptivity to free-stream turbulence. Although there has been solid experimental verification of the linear theory describing acoustic receptivity of boundary layers, this was the first experimental verification of the mechanism behind local receptivity to a convected disturbance. The harmonic wake from a vibrating ribbon positioned upstream of a flat plate provided the free-stream disturbance. Two-dimensional roughness elements on the surface of the plate acted as a local receptivity site. Hot-wire measurements in the boundary layer downstream of the roughness confirmed the generation of Tollmien–Schlichting (TS) instability waves by an outer-layer interaction between the long-wavelength convected disturbance and the short-scale mean-flow distortion due to the roughness. The characteristics of the instability waves were carefully measured to ensure that their behaviour was correctly modelled by linear stability theory. This theory was then used to determine the immeasurably small initial wave amplitudes resulting from the receptivity process, from wave amplitudes measured downstream. Tests were performed to determine the range of validity of the linear assumptions made in current receptivity theories. Experimental data obtained in the linear regime were then compared to theoretical results of other authors by expressing the experimental data in the form of an efficiency function which is independent of the free-stream amplitude, roughness height and roughness geometry. Reasonable agreement between the experimental and theoretical efficiency functions was obtained over a range of frequencies and Reynolds numbers.

---

### 1. Introduction

The receptivity of a laminar boundary layer to a particular type of free-stream disturbance is a measure of the extent to which that disturbance excites instabilities in the boundary layer. Once excited, Tollmien–Schlichting (TS) instability waves grow in accordance with linear stability theory until nonlinear and three-dimensional effects contribute to a breakdown of the flow into turbulence. This path to transition has received a lot of attention in the years since the existence of the TS instability was experimentally confirmed by Schubauer & Skramstad (1948). TS waves are eigenvalues of the Orr–Sommerfeld equation – a fourth-order linear ordinary differential equation derived from the linearized Navier–Stokes equations for parallel flows. Solutions of this equation describe the stability characteristics of the boundary layer. Current transition prediction criteria are based on these solutions and assume that transition will occur when the TS waves have been amplified by an empirically determined  $N$ -factor. These criteria are limited because they are independent of the free-stream

disturbance environment. Measurements have clearly demonstrated that boundary-layer transition is dependent on the amplitude, frequency and type of disturbances present in the free stream. The goal of receptivity analyses is to improve transition prediction methods by extending transition criteria to include the characteristics of the free-stream disturbance environment.

Early receptivity studies such as that by Gaster (1965) were based on the Orr–Sommerfeld equation with local forcing introduced at the boundary. Locally introduced disturbances have energy over a broad spectrum of wavenumbers and are able to couple directly with the boundary-layer instability waves (Kerschen 1989). This type of analysis is relevant to boundary-layer excitation by surface-mounted vibrating ribbons or by unsteady surface suction/blowing. However, free-stream acoustic disturbances, which propagate at the speed of sound, and vortical disturbances, which are convected with the free stream, cannot couple directly with TS waves, which typically propagate at a third of the free-stream velocity. For a given frequency the three will have substantially different wavenumbers and the direct forcing required in the Orr–Sommerfeld solution cannot occur. The central importance of a wavelength conversion mechanism to the natural receptivity problem was recognized by Reshotko (1976).

Early experiments and theoretical analyses concentrated on receptivity mechanisms occurring in the leading-edge region of flat-plate boundary layers. However, for the Blasius boundary layer, waves excited at the leading edge will undergo a sustained period of decay before reaching the lower branch of the neutral stability curve (branch I) where they begin to grow. Numerical calculations by Murdock (1980) and theoretical analyses by Goldstein (1983) and Goldstein, Sockol & Sanz (1983) predicted TS amplitudes at the branch I location of a thin flat plate to be several orders of magnitude less than the free-stream forcing amplitude. Yet Leehey & Shapiro (1980) measured TS waves at the branch I location of their flat plate which were of the same order as the acoustic forcing. In another important experiment, Aizin & Polyakov (1979) demonstrated a separate local receptivity mechanism. They measured an increase in the acoustic receptivity of a flat-plate boundary layer when they introduced a thin surface roughness element in the vicinity of branch I. The receptivity increased linearly with acoustic forcing and with roughness height and was dependent on the width of the roughness strip. A detailed account of this experiment is given in Nishioka & Morkovin (1986).

Goldstein (1985) and independently Ruban (1985) provided theoretical analyses of this local receptivity mechanism. Using triple-deck theory they showed that the local short-scale mean flow distortion due to a small roughness element or a sudden change in surface curvature could produce a strong coupling between the long-wavelength acoustic disturbances and the short-wavelength TS waves. Wavelength conversion results when temporal modulation of the mean-flow distortion, by the acoustic excitation, generates frequency/wavelength combinations which match that of the TS wave (Kerschen 1990). Using this theory, Goldstein was able to obtain good quantitative agreement with the experimental results of Aizin & Polyakov (1979), and Goldstein & Hultgren (1987) were able to show that the site for the increased receptivity in Leehey & Shapiro's experiment was the junction of their leading edge and flat plate. Goldstein's localized acoustic receptivity analysis for small surface variations was extended into the nonlinear regime of large roughness elements by Bodonyi *et al.* (1989), who solved the nonlinear triple-deck equations for the steady flow numerically. They found that the receptivity was linear until the roughness height was of the order of the viscous lower deck of the triple-

deck structure. Larger roughness elements caused a marked increase in receptivity.

An alternative to the asymptotic analyses of localized receptivity was developed independently by Zavol'skii, Reutov & Rybushkina (1983), Choudhari & Streett (1992) and Crouch (1992). For small surface variations, locally parallel flow is assumed to apply and the unsteady flow is expressed as a perturbation of the Orr–Sommerfeld equation rather than the triple-deck equations. At first order, the free-stream disturbance and the mean-flow distortion exist independently, but at second order, the two interact to produce a wave with the frequency of the free-stream disturbance and a wavenumber given by the sum of the free stream and surface wavenumbers. Thus the analysis includes the wavelength conversion mechanism described by Goldstein and Ruban. Although the Orr–Sommerfeld assumption of locally parallel flow at finite Reynolds numbers is not rigorous, this technique is not limited to the Reynolds number and frequency scaling of the lower-branch asymptotic analyses and so the effects of variations in Reynolds number and frequency may be investigated. In this formulation, the receptivity is given by

$$u'_{ts} = u'_{fs} F(\alpha_{ts} - \alpha_{fs}) \mathcal{A}(F, R), \quad (1.1)$$

where  $u'_{ts}$  is the amplitude of the TS wave,  $u'_{fs}$  is the amplitude of the free-stream disturbance and  $F(\alpha_{ts} - \alpha_{fs})$  is the spatial Fourier transform of the surface geometry evaluated at a wavenumber equal to the difference between the TS wavenumber,  $\alpha_{ts}$ , and the wavenumber of the free-stream disturbance,  $\alpha_{fs}$ . This important expression embodies the linear assumptions inherent in the theory and distils the receptivity mechanism into an efficiency function  $\mathcal{A}(F, R)$  which is independent of the surface geometry. The efficiency function proves to be a good vehicle for comparing results of different theoretical calculations and experimental measurements.

The body of these Orr–Sommerfeld-based finite Reynolds number studies is extensive. Results have been obtained for acoustic receptivity at localized and distributed roughness and at short-scale variations in wall suction, porosity and temperature. Hill (1995) obtained a comparable result for local acoustic receptivity by solving the adjoint problem. Detailed reviews are given in Choudhari & Streett (1994) and Crouch (1994*a*). A comparison between finite Reynolds number results and results of calculations using the parabolized stability equations made by Crouch & Bertolotti (1992) for acoustic receptivity and by Lin, Stuckert & Herbert (1995) for vortical receptivity, showed the two methods to be in agreement. A further comparison between the results of finite Reynolds number calculations and those of a direct numerical simulation of acoustic receptivity at localized surface suction made by Crouch & Spalart (1995) also showed good agreement. These comparisons suggest the parallel-flow assumptions made in the Orr–Sommerfeld formulation were valid for the cases considered. Comparisons with results of the asymptotic calculations of Goldstein made by Choudhari & Streett (1992) and Crouch (1992) showed that both calculations followed similar trends with frequency and Reynolds number. The finite Reynolds number results would be expected to approach the asymptotic results in the branch I region at high Reynolds numbers and this appeared to be the case.

A number of experiments on local acoustic receptivity have followed that of Aizin & Polyakov (1979). Wlezien, Parekh & Island (1990) measured the acoustic receptivity at a porous strip. They used hot-wire data from a number of closely spaced vertical profiles measured near the second branch of the neutral stability curve to separate the short-wavelength TS waves from the long-wavelength acoustic waves. A high aspect

ratio leading edge was used to reduce any contribution from leading-edge receptivity and a linear increase in receptivity with acoustic forcing was observed. Saric, Hoos & Radeztsky (1991) investigated the linearity of acoustic receptivity with roughness height. Their measurements confirmed the finding of Bodonyi *et al.* (1989) that the onset of nonlinearity occurs when the roughness exceeds the viscous lower deck. Wiegel & Wlezien (1993) measured acoustic receptivity at a wavy wall simulated by an array of surface roughness elements. They showed that the receptivity at distributed roughness was an order of magnitude greater than receptivity at local roughness and that there was strong tuning about the resonant condition when the TS wavenumber matched the wall wavenumber. Their results agreed well with those of finite Reynolds number calculations by Choudhari & Streett (1992). Zhou, Liu & Blackwelder (1994) measured acoustic receptivity to two- and three-dimensional roughness elements and demonstrated the dependence of the local receptivity on the spatial Fourier transform of the surface roughness as well as confirming other aspects of the acoustic receptivity theory. Breuer *et al.* (1996) investigated receptivity to broad-band acoustic forcing at surface roughness and demonstrated a linear variation with the height and number of roughness elements.

The theory of receptivity to vortical disturbances is as well developed as that for acoustic disturbances. One of the first analyses of the response of a boundary layer to convected vorticity was carried out by Rogler & Reshotko (1975). They modelled the free-stream disturbance as a convected array of counter-rotating harmonic vortices. It was a forced problem because without a receptivity site there was no mechanism for wavelength conversion. Results of their calculations showed that the disturbances were highly damped near the wall with most of the energy confined to the outer part of the layer. This is quite different from the disturbance profile associated with an acoustic disturbance which has the profile of a Stokes shear wave with significant energy close to the wall.

Kerschen (1989) used asymptotic methods to analyse the local receptivity to vortical disturbances. He identified a vortical receptivity mechanism quite different from that of acoustic receptivity. While acoustic receptivity arises from an interaction between the Stokes wave and the mean-flow distortion in the viscous lower deck, vortical receptivity arises from an interaction between the vortical disturbance and the short-scale mean-flow distortion in the upper deck. The efficiency function  $A(F, R)$  calculated by Kerschen (1990) for vortical receptivity was an order of magnitude less than that calculated by Goldstein (1985) for acoustic receptivity. (The  $\epsilon$  factor in Kerschen's receptivity expression is included in his vortical receptivity efficiency function in this comparison.) Kerschen (1991) included a second-order effect in his calculation of vortical receptivity, due to pressure fluctuations in the base flow which bring the acoustic receptivity mechanism into play. This effect causes the receptivity to vary with the convection speed of the vortices, reaching a minimum when the convection speed is 0.94 times the free-stream velocity, and approaching the value for an acoustic wave as the speed is increased.

Zavol'skii *et al.* (1984) used the Orr–Sommerfeld-based finite Reynolds number technique to calculate the receptivity of a flat-plate boundary layer over a small-amplitude periodically wavy wall to vortical disturbances. The vortical disturbance modelled was the wake from a vibrating ribbon convected above the boundary layer. A Gaussian profile was assumed for the unsteady stream function describing the wake. They noted that the most effective TS wave excitation occurs at the resonance condition  $\alpha_{wall} = \alpha_{ts} - \alpha_{fs}$ , where  $\alpha_{wall}$  is the wavenumber of the surface roughness. They also noted that the boundary layer is most sensitive to distributed roughness at

the branch I location as waves excited at this location experience the maximum subsequent growth. Choudhari (1994) presented a parametric study of the local receptivity of a boundary layer to convected vorticity. Following Zvol'skii *et al.*, Choudhari assumed that the free-stream disturbance was a harmonic wake with a Gaussian profile. Crouch (1994*a, b*) analysed vortical receptivity at local and distributed surface suction and roughness. He adopted the convected array of vortices studied by Rogler & Reshotko (1975) as a representative free-stream disturbance. His calculations were referenced to the free-stream vortex strength and the resulting receptivity coefficient was dependent on the position of the vortices relative to the plate surface. Choudhari (1996) analysed the response of a boundary layer to two- and three-dimensional gusts and calculated the local receptivity to these gusts at two-dimensional roughness.

Despite the strong theoretical backing for receptivity to convected disturbances, there has been little experimental verification for this class of disturbance. The experiment of Kachanov, Kozlov & Levchenko (1978) concentrated on the leading edge, and with no receptivity sites aft of this region, no TS wave generation was observed downstream of the leading edge. In a later experiment, Parekh, Pulvin & Wlezien (1991) investigated the receptivity to vortical disturbances at a backward-facing step. Their disturbance was a non-compact gust generated by vibrating an array of ribbons upstream of the plate leading edge. No vortical receptivity was detected in this experiment. It was suggested that this may have been due to the convection speed of the wake which was estimated to be slightly less than the free-stream velocity. Kerschen (1991) calculated reduced receptivity for such a convection speed. In addition the spatial Fourier transform of a step is not as great as a roughness element of resonant width. In his analysis of vortical receptivity, Choudhari (1994) asserted that a properly designed experiment, using a convected wake over distributed roughness, would produce measurable TS waves and he quantified many of the parameters involved in designing such an experiment.

An experimental investigation of localized boundary-layer receptivity to a convected disturbance is reported in this paper. The experimental set-up and some preliminary results were originally reported in Dietz (1996). The wake from a vibrating ribbon was chosen as the free-stream disturbance in line with Choudhari's recommendations. The experiment was designed with attention to the advice of Nishioka & Morkovin (1986) and Saric (1990) regarding receptivity experiments. In particular, care was taken to ensure that a Blasius mean flow with linear stability characteristics was established on the flat plate, and that all uncontrolled disturbances with the potential to excite the boundary layer were minimized. The experimental arrangement is outlined in §2. The results reported in §3 include measurements of the mean flow, the free-stream disturbance and the boundary-layer instability waves. These measurements confirmed that linear stability theory correctly modelled the experimental instability waves, and that this theory could be used to determine the immeasurably small initial wave amplitudes from wave amplitudes measured downstream. A series of tests establishing the range of validity of the linear assumptions in (1.1) are also reported in §3. This equation was then used to determine the receptivity efficiency function over a range of excitation frequencies and roughness Reynolds numbers from measurements of the TS wave amplitude. In §4, the trends evident in the experimental data are shown to compare favourably with those of the theory. Experimental verification of the mechanism behind local receptivity to convected vortical disturbances is a step towards understanding local receptivity to free-stream turbulence and towards developing a transition criterion based on free-stream disturbance levels.

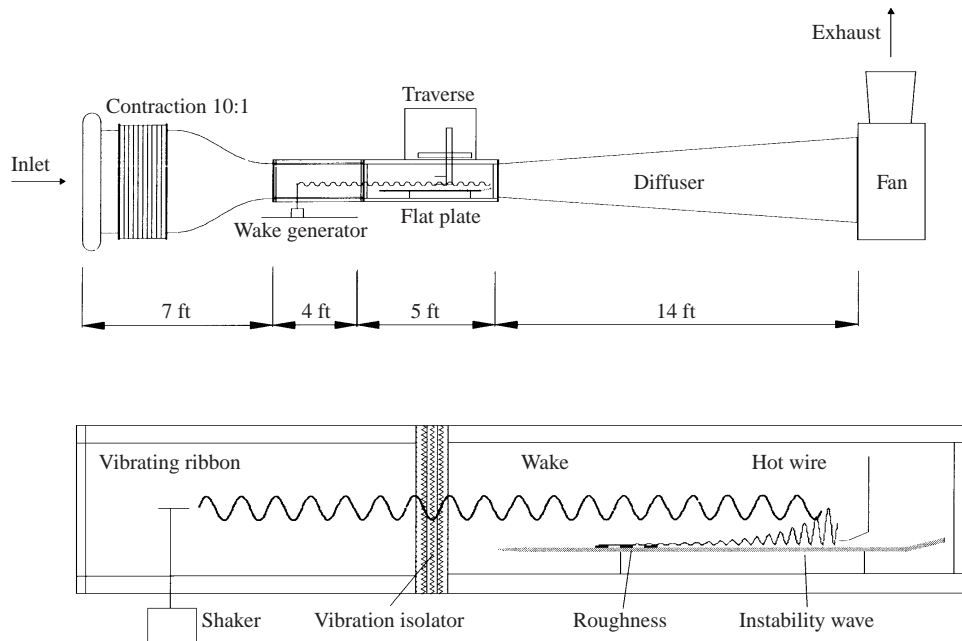


FIGURE 1. Experimental set-up showing the excitation of two-dimensional TS waves by the interaction between a long-wavelength harmonic disturbance convected in the wake from a vibrating ribbon and a short-scale mean-flow distortion due to surface roughness. The waves are measured downstream using a traverse-mounted hot wire.

## 2. Experimental arrangement and measurement technique

The experiment was carried out in a low-speed indraft wind tunnel in the Fluid Mechanics Laboratory at the NASA Ames Research Center. A schematic of the experimental apparatus is given in figure 1. The tunnel has a 0.4 m square  $\times$  2.6 m long test section and is powered by a centrifugal blower. A settling chamber, with honeycomb and eight seamless fine-mesh screens followed by a 10:1 contraction, results in a high-quality test section flow with non-uniformity below 0.5%, angularity below  $0.3^\circ$  and a turbulence intensity in the range 3 Hz to 10 kHz of 0.07%.

Measurements were made on a highly polished flat plate with a 58:1 elliptic leading edge. The high aspect ratio leading edge was chosen to minimize leading-edge effects. The plate was mounted horizontally near the centre of the test section on vibration-isolation supports. Foam seals were fitted along each side of the plate to prevent leakage between the upper and lower surfaces. A 12.7 mm wide  $\times$  51  $\mu$ m thick ribbon mounted 0.58 m ahead of the plate leading edge was used to introduce the convected disturbance. The ribbon was stretched between two shafts mounted in sealed enclosures on either side of the test section. A single electromagnetic shaker was used to drive the shafts. The ribbon was tensioned until its first natural frequency was well above the desired forcing frequency so that a two-dimensional wake would result without any contributions from higher ribbon vibration modes. Roughness elements were constructed from strips of  $50 \pm 2$   $\mu$ m thick polyester tape, 25.4 mm wide.

Velocity measurements were made using two single-wire Dantec 5  $\mu$ m diameter platinum-plated tungsten hot-wire probes. Only single-wire probes were used in this investigation so all reported velocity measurements are of the streamwise velocity. The

primary probe was supported by a three-axis traverse housed in a sealed enclosure above the test section. A streamlined sting passed from the traverse enclosure, through a sealed slot, into the test section where the hot wire was mounted at the tip of a 0.12 m long extension tube to ensure it was free from any pressure-gradient effects associated with the sting. An electrical contact at the base of the sting was used to locate the plate at the start of each boundary-layer profile measurement. Care was taken to minimize any vortex shedding from the sting or the slot which could corrupt the measurements. A second hot wire was used as a reference for phase measurements. It was mounted on a fixed sting at the streamwise location of branch I. The wire was offset 0.05 m in the spanwise direction from the tunnel centreline and positioned just above the stationary ribbon's wake. Free-stream pressure was measured with a pitot tube mounted on the traverse sting 30 mm above the primary hot wire. Free-stream temperature was measured with a platinum-resistance thin film detector also mounted on the traverse sting. Atmospheric pressure was regularly updated from a digital barometer.

The hot wires were always calibrated at the same reference positions against free-stream velocity determined from the pitot tube. Temperature sensitivity was reduced by assuming the following function based on the rate of heat transfer from the wire:

$$U = f \left( \frac{E_w}{(T_w - T_{fs})^{1/2}} \right), \quad (2.1)$$

where  $U$  is the streamwise velocity at the wire,  $E_w$  is the wire voltage,  $T_{fs}$  is the free-stream temperature and  $T_w$  is the wire temperature calculated assuming  $T_w = (R_w - 1)/\alpha_0 + T_0$ , where  $R_w$  is the wire overheat ratio, set at 1.8 for these experiments, and  $\alpha_0 = 0.0036$  is the temperature coefficient of resistivity of the wire at a reference temperature  $T_0$  of 293 K. An eight-point fourth-order polynomial fit was used with calibration velocities distributed to give more points in the low-velocity region where the calibration curve had the greatest variation. The calibration's 95% confidence limits were typically  $\pm 0.05 \text{ m s}^{-1}$  which is 0.3% of the free-stream velocity. The wires were calibrated before every measurement sequence and possible drift in the calibration was checked on completion of the sequence. If the difference between the velocity from the hot wire and that from the pitot tube was greater than 3% the calibration and measurement sequence were repeated. However, the drift was typically less than 1% of the free-stream velocity. After each test, the measured profiles were inspected using a graphical interface. During this inspection, near-wall data points obviously affected by heat conduction to the wall were discarded. The wall location was then determined from a linear extrapolation of the near-wall velocities.

All analogue signals were acquired simultaneously by a high-speed 15 bit Tustin A/D converter and then transferred to a MicroVAX II computer. Ten blocks of 5000 samples acquired at 2500 Hz were recorded at each point. The signal from the traverse hot wire was low-pass filtered at 10 kHz and recorded on one channel for the mean velocity, and further high-pass filtered at 3 Hz and recorded on a separate channel for the velocity fluctuations. The high-pass filtering was required to remove low-frequency unsteadiness, associated with a suspected separation in the diffuser, from the velocity fluctuation measurements. The r.m.s. amplitude of the velocity fluctuations was estimated from the product of the a.c. coupled r.m.s. voltage and the local slope of the d.c. calibration curve. Spectral measurements were performed with a HP3665A Dynamic Signal Analyzer. The component of the velocity fluctuations at the ribbon forcing frequency was obtained from a power spectrum of the hot-wire signal. The phase of this component was obtained from a cross-spectrum between the

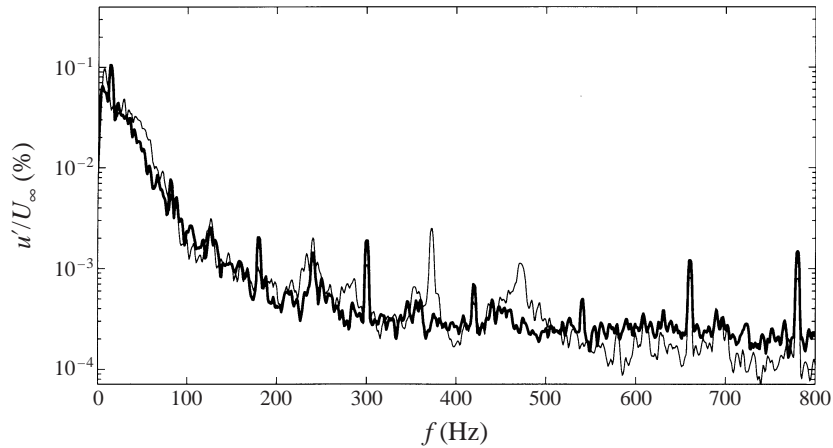


FIGURE 2. Turbulence intensity spectrum measured in the boundary layer (shown in bold) and the free stream.  $x = 0.71$  m,  $R = 910$ .

traverse hot-wire signal and the reference hot-wire signal. These measurements were recorded after 12 ensemble averages. A flat-top window with a bandwidth of 3.82 Hz was used.

As the TS waves at branch I were too small to be accurately measured, the waves were measured at a downstream location where the exponential growth of the waves had increased their amplitudes to measurable levels. The parameters of the experiment were optimized for resonance with roughness elements of a certain width positioned at branch I, and for maximum amplification from this site to the downstream measurement position. The downstream position was fixed at 0.71 m from the leading edge as sidewall contamination was unacceptable aft of this position. The theory reported in § 1 suggested that the most effective TS wave excitation would occur at the resonance condition,  $\alpha_{wall} = \alpha_{ts} - \alpha_{fs}$ . For standard 25.4 mm tape, these constraints resulted in an optimum frequency parameter of  $F = 2\pi f\nu/U_\infty^2 \times 10^6 = 50$  where  $f$  is the ribbon forcing frequency,  $\nu$  is the dynamic viscosity and  $U_\infty$  is the free-stream velocity. The optimum branch I Reynolds number was  $R_I = (U_\infty x/\nu)^{1/2} = 613$ , where  $x$  is the streamwise distance from the virtual leading edge (§ 3.1). These parameters give  $U_\infty = 17$  m s<sup>-1</sup> and  $f = 157$  Hz at a reference temperature of 288 K and a reference dynamic viscosity of  $1.455 \times 10^{-5}$  m<sup>2</sup> s<sup>-1</sup>. The experiment was controlled to maintain constant  $R$  and  $F$  by adjusting the free-stream velocity and the ribbon forcing frequency as the flow temperature and the atmospheric pressure varied from the reference values.

### 3. Results

#### 3.1. Base flow

Receptivity experiments are best realized by minimizing all uncontrolled background disturbances. A controlled disturbance may then be introduced and its effect on the boundary layer measured. The tunnel used for this experiment has a satisfactory turbulence intensity (below 0.1%). This measure is a combination of free stream turbulence and flow unsteadiness due to the blower. The tunnel has a large blower operating well below its design point. This proved to be advantageous as shown in the streamwise velocity spectrum given in figure 2. The fan speed was less than



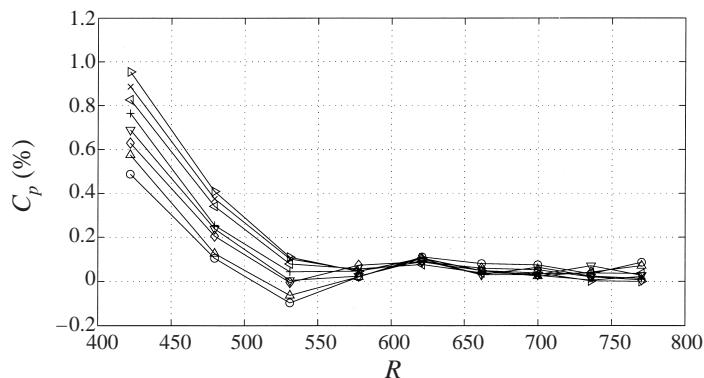


FIGURE 3. Pressure coefficient measured at the following heights above the plate surface:  $y = 14$  mm ( $\circ$ ), 20 mm ( $\triangle$ ), 26 mm ( $\diamond$ ), 31 mm ( $\nabla$ ), 37 mm ( $+$ ), 43 mm ( $\triangleleft$ ), 48 mm ( $\times$ ), 54 mm ( $\triangleright$ ).

10 Hz which with eight blades resulted in a blade passing frequency which was less than 80 Hz. With the fan unsteadiness contained at low frequencies, the disturbance levels in the frequency range of interest, 110–220 Hz, were of the same order as the electrical noise in the signal. The spanwise variation of the streamwise velocity was also measured to ensure that results would not be corrupted by three-dimensionality in the base flow. The fluctuation levels in the boundary layer remained below 0.1% of the free-stream velocity in the region  $\pm 2.5$  cm of the centreline until sidewall contamination became significant at  $x = 0.71$  m.

A zero pressure gradient (Blasius) boundary layer was established on the upper surface of the flat plate by setting the plate at a slight angle of attack to counter the effects of the growing boundary layers on the plate surface and the tunnel walls. The pressure gradient in the leading-edge region was further modified by adjusting a flexible ceiling in the test section to minimize the adverse pressure gradient at the leading-edge/plate juncture, which was just upstream of branch I. The final pressure gradient obtained after an iterative adjustment procedure is shown in figure 3 where the pressure coefficient is plotted against streamwise distance at a number of heights above the plate surface. The coefficient was obtained by dividing the differential pressure between the traverse static port and a wall static port located well upstream of the leading edge, by the dynamic pressure measured at a fixed reference location. Measurements within 10 mm of the wall were affected by a wall proximity error and are not reported. The variation in pressure coefficient was within  $\pm 0.2\%$  for  $R > 520$  and was less than  $\pm 0.1\%$  for  $R > 600$ . The leading-edge region,  $R < 520$ , had a strong favourable pressure gradient which was considered to be beneficial as it served to dampen any instabilities excited at the leading edge. After each adjustment of the pressure gradient, a flap at the rear of the plate was used to move the stagnation point back to the tip of the leading edge. The location of the stagnation point was inferred from surface static-pressure measurements made on either side of the plate, 25 mm from the leading edge, using miniature static-pressure probes taped to the plate surface.

The Blasius character of the boundary layer was confirmed from profiles of the mean streamwise velocity recorded at a number of  $x$ -stations. The shape factor calculated from these profiles was consistently within 1% of the Blasius value of 2.59. A virtual origin for the boundary layer was also calculated from these profiles:

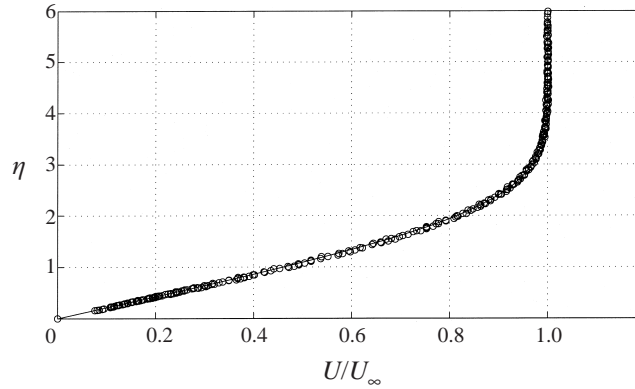


FIGURE 4. Profiles of the mean streamwise velocity in the boundary layer at 12 stations from  $R = 630$  to  $R = 900$ , plotted against the boundary-layer coordinate  $\eta = y/(2\nu x/U_\infty)^{1/2}$  and compared with the theoretical Blasius profile.

$x_{vo} = \delta^*{}^2 U_\infty / (1.728\nu)$ . The virtual origin for this experiment was estimated to be 0.025 m aft of the physical leading edge. All  $x$ -data reported in this paper are referenced to this virtual origin. A comparison of the mean-velocity profiles with the theoretical Blasius profile is given in figure 4 using the non-dimensional height  $\eta = y/(2\nu x/U_\infty)^{1/2}$ . The measurements, recorded at 12 stations from  $R = 630$  to  $R = 900$ , confirm the self-similarity of the profiles and the accuracy of the virtual origin.

### 3.2. Convected disturbance

Detailed measurements were made of the harmonic disturbance convected with the wake from the ribbon to establish the input to the receptivity process. The ribbon was set well ahead of the plate leading edge to ensure a small wake deficit and hence minimize the nonlinear effects calculated by Kerschen (1991), whose results suggested the receptivity would decrease as the disturbance convection speed decreased, reaching a minimum at  $0.94U_\infty$ . Plots of the mean streamwise velocity,  $U$ , and of the r.m.s. velocity fluctuations,  $u'$ , in the boundary layer and the ribbon wake with no ribbon vibration are given in figure 5. The velocity deficit in the wake was less than 2% of the free-stream velocity which indicates that the disturbance convection speed was close to the free-stream value. The wake's Gaussian mean-flow deficit is located well outside of the boundary layer and the turbulence intensity, which has a maximum of 0.45% in the wake, decays to negligible values before the edge of the boundary layer. A plot of the component of the velocity fluctuations at the ribbon forcing frequency of 157 Hz is also included in the figure. With no ribbon vibration, this component remains below 0.03% in the wake and there is no detectable excitation of the boundary layer at this frequency. These measurements suggest the turbulence in the wake is sufficiently removed from the boundary layer and will not affect the receptivity measurements.

Profiles of the wake with the ribbon vibrating are given in figure 6. Both narrow-band (157 Hz) and broad-band (3–10 kHz) fluctuations are included in the figure. The narrow-band fluctuations at the forcing frequency dominate the profile and extend well beyond the turbulent region of the wake. The presence of the plate causes a plateau in the fluctuation level at the boundary-layer edge, where there is little change in the fluctuation level from  $\eta = 6$  to 12. Inside the boundary layer the

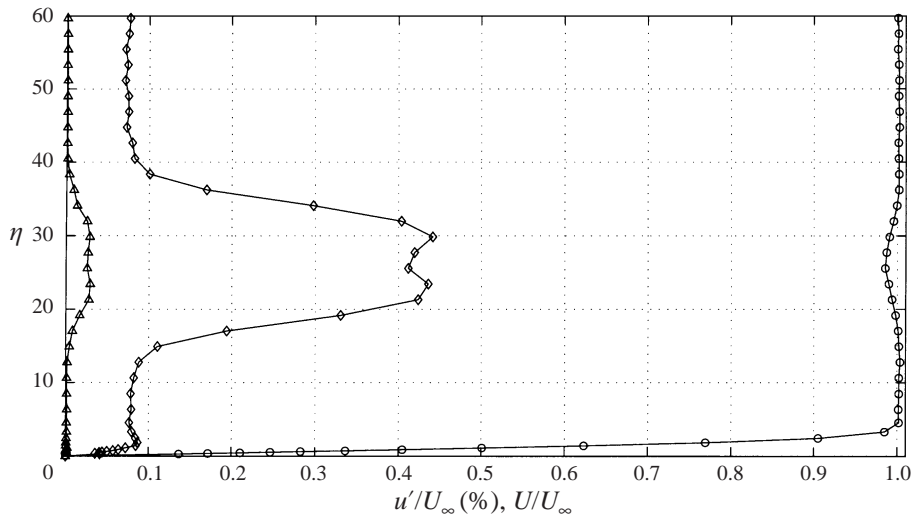


FIGURE 5. Profile of the streamwise velocity in the boundary layer and the wake behind the stationary ribbon measured at  $R = 633$ . Broad-band r.m.s. fluctuations  $u'/U_\infty$  from 3 Hz to 10 kHz ( $\diamond$ ), component of  $u'/U_\infty$  at 157 Hz ( $\Delta$ ), mean velocity  $U/U_\infty$  ( $\circ$ ).

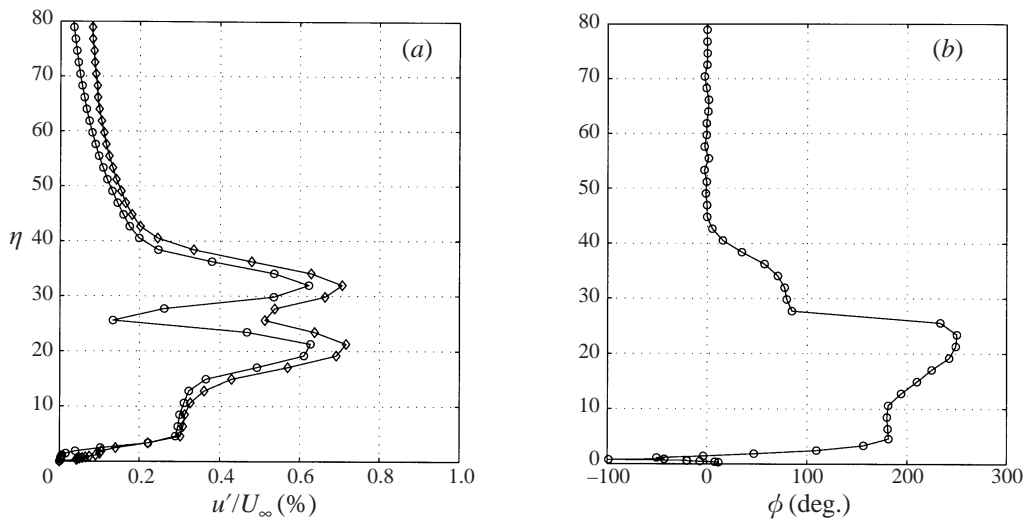


FIGURE 6. Profiles of the amplitude (a) and phase (b) of the streamwise velocity fluctuations measured in the boundary layer and the wake behind the vibrating ribbon.  $R = 633$ ,  $F = 50$ . Broad-band r.m.s. fluctuations  $u'/U_\infty$  from 3 Hz to 10 kHz ( $\diamond$ ), component of  $u'/U_\infty$  at ribbon forcing frequency of 157 Hz ( $\circ$ ).

fluctuations rapidly decay to zero at the wall. A plot of the phase of the fluctuations is also given in figure 6 showing a  $180^\circ$  phase change in the centre of the wake and rapid variation in the boundary-layer region. The amplitude and phase profiles are similar to those measured by Wygnanski, Champagne & Marasli (1986) in their study of instabilities in small-deficit turbulent wakes. Wygnanski *et al.* also calculated a linearized Navier–Stokes solution which was in good agreement with the results of their measurements.

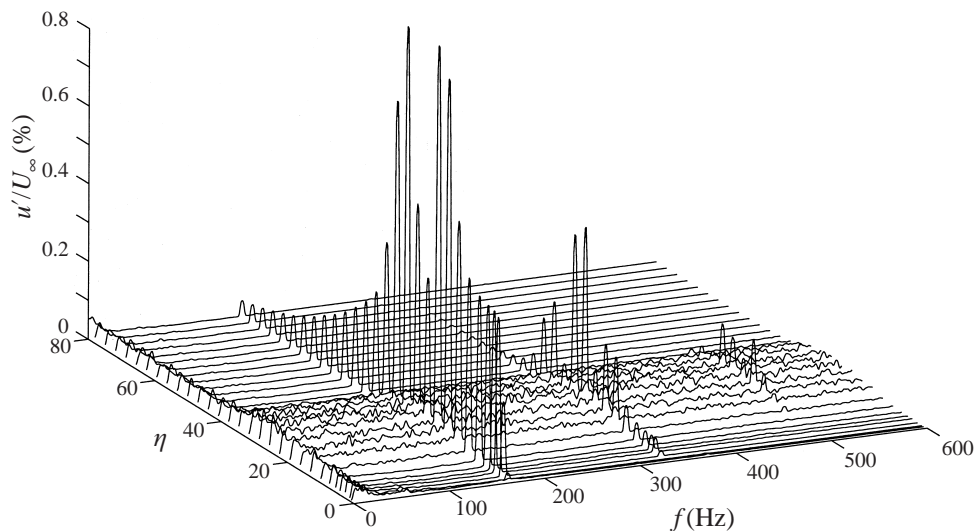


FIGURE 7. Streamwise velocity spectra recorded in the boundary layer and the wake behind the vibrating ribbon.  $R = 633$ ,  $F = 50$ .

A plot of streamwise velocity spectra recorded at points through the boundary layer and the vibrating ribbon wake is given in figure 7. The broad-band turbulence in the wake is centred at  $\eta = 25$  as expected from the profile of the wake from the stationary ribbon shown in figure 5. While the turbulent fluctuations are localized in the wake well above the boundary layer, fluctuations at the forcing frequency extend into the potential flow region outside the wake and excite the boundary layer. Some energy is present in the second and third harmonics of the forcing frequency but tensioning the ribbon has reduced these harmonics to acceptable levels. These measurements illustrate that the wake from a vibrating ribbon is an effective way to excite a boundary layer with single-frequency convected disturbances.

The disturbance profile inside the boundary layer is shown in figure 8 where the real and imaginary parts of the amplitude of the streamwise velocity fluctuations are plotted. As predicted by Rogler & Reshotko (1975), most of the disturbance energy is confined to the outer part of the boundary layer and the fluctuations are rapidly damped towards the wall. Profiles recorded at different streamwise locations (not plotted here) show that the penetration of the disturbance into the boundary layer decreases as  $R$  increases. A similar trend was found by Choudhari (1996) in his calculations of the response of a boundary layer to a two-dimensional gust. Choudhari, and also Davis (1997), calculated a numerical solution of the linearized unsteady boundary-layer equations with streamwise forcing as the upper boundary condition. Their results are in agreement and as shown in figure 8, closely match the measured disturbance profile. The agreement between the measured profile and the calculated profile is important as this profile is the input into the receptivity process, and the accuracy of any receptivity calculation will depend on the accuracy of the calculated boundary-layer disturbance profile.

The degree to which these calculations model the response of the boundary layer suggests that the boundary-layer response is primarily determined by the streamwise forcing at its edge. This hypothesis was tested experimentally by varying the wake height while keeping the wake amplitude at the boundary-layer edge constant. The result is shown in figure 9(a). Although the wake profiles are dissimilar, with the

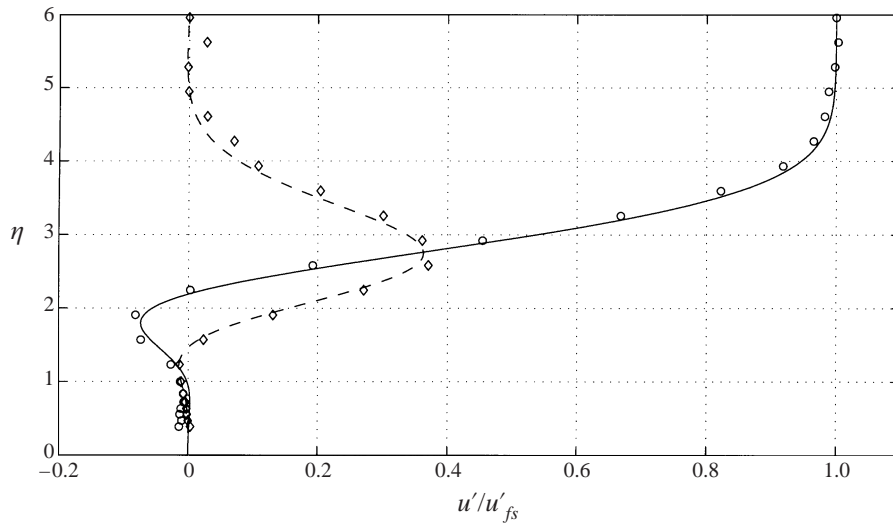


FIGURE 8. Complex amplitude of the convected disturbance measured in the boundary layer at  $R = 630$ : real part ( $\circ$ ), imaginary part ( $\diamond$ ). Numerical solution of the linearized unsteady boundary layer equations with streamwise forcing as the upper boundary condition: real part (—), imaginary part (---). Numerical results from Choudhari (1996) and Davis (1997). All data are referenced to the values at the edge of the boundary layer.

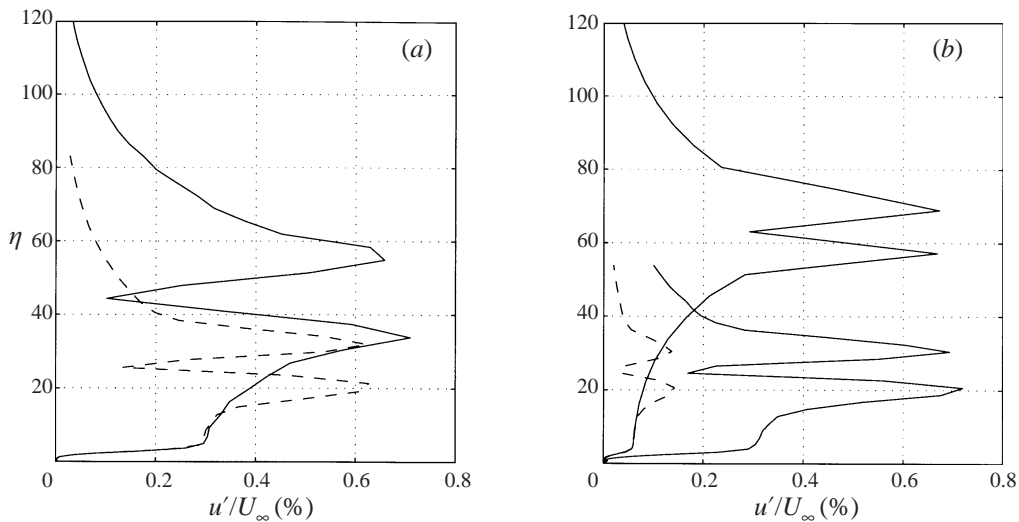


FIGURE 9. Effect of wake height on the disturbance profile in the boundary layer. (a) Ribbon was moved from  $\eta = 45$  (—) to  $\eta = 25$  (---). Ribbon vibration amplitude was set to keep the fluctuation amplitude at the edge of the boundary layer constant at  $u'_{fs}/U_{\infty} = 0.3\%$ . (b) Ribbon was moved from  $\eta = 63$  to  $\eta = 25$ . Ribbon vibration amplitude was kept constant. Dashed line is the lower profile scaled by  $e^{\alpha_{fs}(y_1 - y_2)}$  where  $\alpha_{fs}$  is the wavenumber of the wake disturbance and  $(y_1 - y_2)$  is the difference in wake heights.

upper wake at a higher level of forcing, the disturbance profile in the boundary layer is the same. The fluctuation amplitude at the edge of the boundary layer,  $u'_{fs}$ , therefore seems to be a good reference measure of the strength of the free stream forcing. This reference location is also attractive in as much as the plateau in fluctuation levels

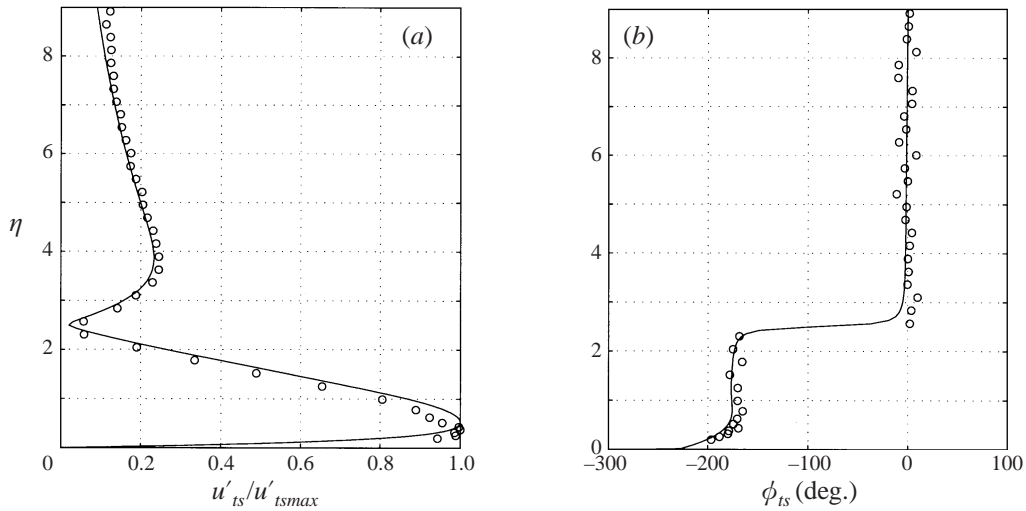


FIGURE 10. Amplitude and phase of the measured TS wave ( $\circ$ ), compared with the eigenvector calculated from linear stability theory (—). Amplitude profiles are normalized by the maximum amplitude ( $u'_{ts}/U_\infty = 0.9\%$ ), phase is referenced to the phase at the edge of the boundary layer.  $R = 900$ ,  $F = 50$ ,  $u'_{fs}/U_\infty = 0.3\%$ . Array of 10 roughness elements, each 25.4 mm wide, 100  $\mu\text{m}$  thick, spaced 50.8 mm apart about  $R_f = 613$ .

at the boundary-layer edge reduces the sensitivity of measurements to small height differences (figure 6).

It can be shown that the fluctuations in an unbounded free stream outside the viscous wake region scale exponentially with the product of the streamwise wavenumber and the distance from the wake centreline. Assume that in the irrotational flow outside the viscous wake, streamwise fluctuations satisfy a stream function of the form  $\Psi = f(y)e^{i(\alpha_{fs}x - \omega t)}$ . Then  $\nabla^2\Psi = 0 \Rightarrow f''(y) = \alpha_{fs}^2 f(y)$  which has the solution  $f(y) = C_1 e^{\alpha_{fs}y} + C_2 e^{-\alpha_{fs}y}$ . The condition  $u' = \partial\Psi/\partial y = 0$  at  $y = -\infty$  gives  $C_2 = 0$  in the region below the wake. Hence the exponential decay of streamwise velocity fluctuations below the wake is given by  $u'_1/u'_2 = e^{\alpha_{fs}(y_1 - y_2)}$ . Although derived for an unbounded flow, this scaling also seems to apply to the potential flow region above the boundary layer when the flow beneath the wake is bounded by the plate. The scaling was confirmed experimentally by measuring the disturbance profile with the ribbon at two heights but with the same vibration amplitude. When the lower profile is scaled by this exponential relationship, it overlays the upper profile in the boundary-layer region (figure 9b). Although the amplitude of the boundary-layer edge forcing is related to the wake disturbance amplitude by this scaling, it is still advantageous to use the edge forcing amplitude as the reference excitation amplitude as this removes the need for a wake-height parameter in the receptivity analysis.

### 3.3. Boundary-layer instabilities

When roughness was added to the plate surface at branch I, the boundary layer did become receptive to the convected disturbance. The receptivity increased with the number of roughness elements on the plate, and with a distributed array of roughness elements a large response was obtained. The mode shape of the instability wave excited by the interaction between the surface roughness and the convected disturbance was determined by a vector subtraction of the profile measured above a smooth plate from a similarly measured profile with roughness on the plate. The

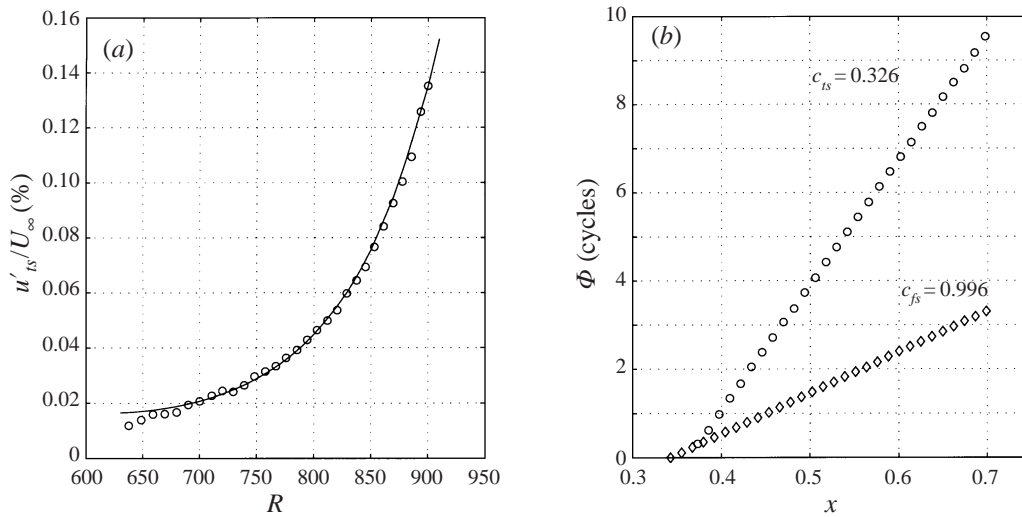


FIGURE 11. (a) Streamwise growth of the measured TS wave ( $\circ$ ), compared with linear stability theory ( $—$ ). (b) Measured phase of the TS wave ( $\circ$ ), and of the wake disturbance ( $\diamond$ ), plotted against streamwise distance.  $F = 50$ ,  $u'_{fs}/U_\infty = 0.3\%$ . Single roughness element, 25.4 mm wide, 100  $\mu$ m thick, at  $R_r = 613$ .

profile so obtained is shown in figure 10. The r.m.s. amplitude profile is normalized by the maximum amplitude and the phase profile is referenced to the phase at the edge of the boundary layer. The measured mode shapes agree with the shape of the TS eigenvector calculated using the  $e^{Malik}$  quasi-parallel stability code (Malik 1989), confirming that the measured instability is a TS wave.

The growth rate and phase speed of the TS waves, shown in figure 11, also closely match the predictions of linear stability theory. The experimental amplitude plotted here is the amplitude measured at a height corresponding to the maximum of the calculated eigenvector at each Reynolds number. At  $R = 625$  this maximum occurs in the boundary layer at  $U/U_\infty = 0.25$  and it moves outward to  $U/U_\infty = 0.4$  at  $R = 920$ . Again, the r.m.s. amplitudes shown result from the vector subtraction of the no-roughness measurement from the roughness measurement. Prior to this subtraction, the roughness amplitudes showed a marked oscillation with streamwise distance due to interference between the TS waves and the convected disturbance. Even after the free-stream disturbance has been subtracted, there is still some oscillation in the amplitudes measured at Reynolds numbers less than 750. This is a consequence of the small wave amplitudes at locations close to the roughness, and it shows why measurements were made at downstream locations where the waves had been amplified. The TS phase speed of  $0.326U_\infty$  agrees well with the theoretical value which varies from 0.32 to 0.33 between the two branches of the neutral stability curve. The measured speed of the convected disturbance was within 1% of the free-stream velocity. This was consistent with the wake deficit, which earlier measurements showed to be less than 2% of the free-stream velocity. Hence, the reduction in receptivity calculated by Kerschen (1991) for decreased convection speeds was avoided in this experimental set-up.

The mode shape, phase speed and growth rate of the measured instability indicate that it is behaving in the manner predicted by linear stability theory and therefore it should be reasonable to use linear stability theory to calculate initial TS amplitudes from the larger, measurable amplitudes at downstream locations. The last question to

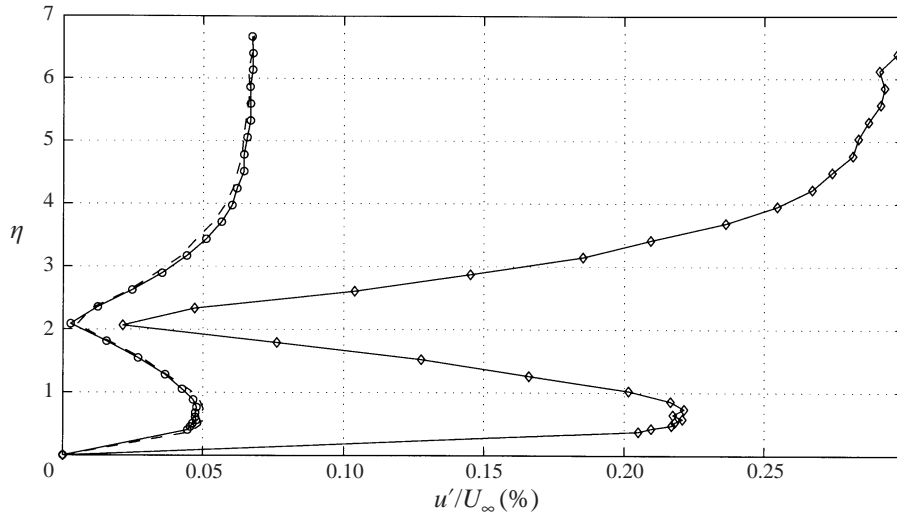


FIGURE 12. Profiles of the streamwise fluctuations in the boundary layer at the ribbon forcing frequency with the ribbon vibrating with constant amplitude but positioned at two heights above the plate: 25 mm ( $\diamond$ ), 50 mm ( $\circ$ ). Dashed line is the 25 mm ribbon profile scaled to give the same fluctuation amplitude at the edge of the boundary layer as the 50 mm ribbon profile.  $R = 850$ ,  $F = 50$ . Array of seven roughness elements, each 25.4 mm wide, 50  $\mu\text{m}$  thick, spaced 50.8 mm apart about  $R_l = 613$ .

be answered regarding the validity of the experiment is whether the instability wave was excited solely by the convected disturbance, or whether there were contributions from acoustic and vibration sources. To differentiate between excitation sources, TS wave amplitudes were measured with the vibrating ribbon positioned at two heights. An accelerometer on the ribbon mounting block was used as a reference to ensure that the ribbon's vibration amplitude remained constant. The two measured profiles are shown in figure 12. When the profile measured with the ribbon in the lower position is scaled by the ratio of the fluctuation levels at the edge of the boundary layer, the resulting boundary-layer profile matches the boundary-layer profile excited by the higher wake. As the ribbon's vibration amplitude was constant, the acoustic and vibration fields were unchanged between the two measurements. Therefore, the fact that the TS amplitude scales with the forcing at the edge of the boundary layer demonstrates that receptivity to convected vorticity was the dominant mechanism generating the measured TS waves.

#### 3.4. Receptivity to convected disturbances

A series of tests was then performed to establish the range of validity of the receptivity expression (1.1). For each configuration, measurements of the maximum TS amplitude in the boundary layer were made at a number of streamwise locations from  $R = 800$  to  $R = 900$ . At each location, the measurement with roughness on the plate was followed by a no-roughness measurement. TS amplitudes were determined from a vector subtraction of the no-roughness amplitude from the roughness amplitude. Estimates of the initial r.m.s. wave amplitude at the roughness location,  $u'_{ISR}$ , were then determined from the TS amplitudes measured downstream,  $u'_{IS}$ , using  $N$ -factors obtained from linear stability calculations using the  $e^{Malik}$  code. Each  $N$ -factor was calculated by integrating the wave growth rate,  $\alpha_i$ , between the Reynolds number of



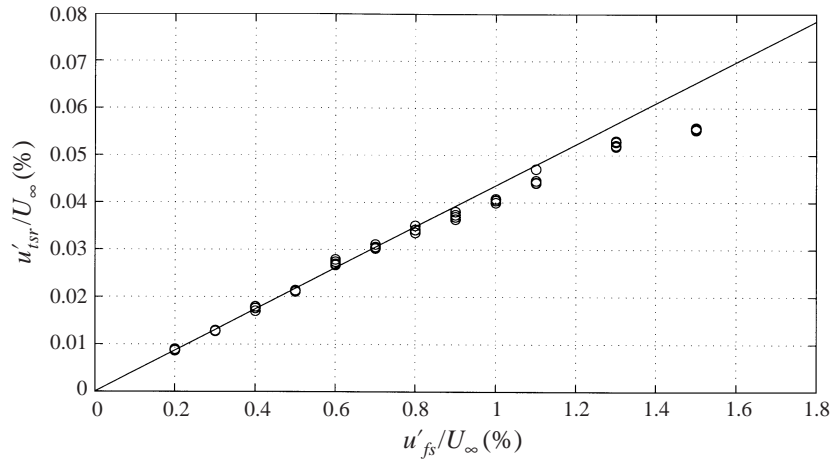


FIGURE 13. Variation of TS amplitude with free-stream forcing amplitude.  $F = 50$ . Single roughness element, 25.4 mm wide, 100  $\mu\text{m}$  thick, at  $R_r = 620$ .

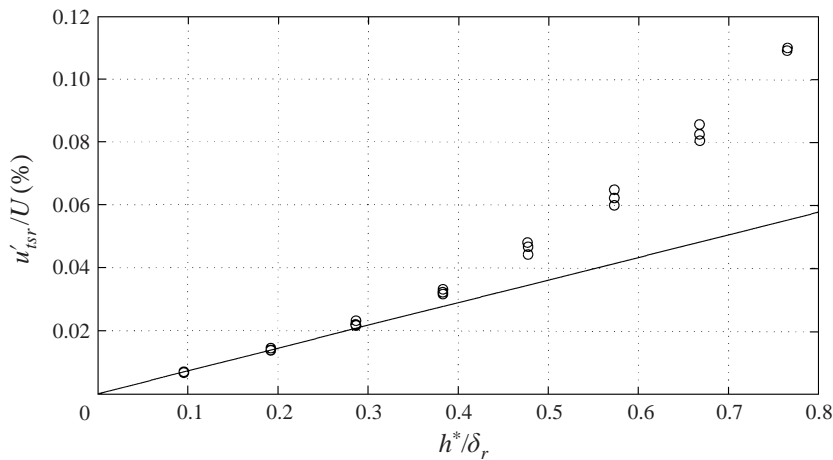


FIGURE 14. TS amplitude variation with non-dimensional roughness height. Boundary-layer reference length  $\delta_r = (\nu x/U_{\infty})^{1/2}$ .  $F = 50$ ,  $u'_{fs}/U_{\infty} = 0.3\%$ . Single roughness element 25.4 mm wide at  $R_r = 620$ .

the roughness location,  $R_r$ , and the Reynolds number of the measurement location,  $R$ .

$$u'_{tsr} = u'_{ts} e^{-N}, \quad N = \int_{R_r}^R -2\alpha_i dR. \quad (3.1)$$

In some cases the roughness was positioned forward of branch I and so both positive and negative growth rates were included in the integration. The degree to which the initial amplitude estimates from different downstream locations collapse onto a single point is a measure of the applicability of the theoretical growth rates to the experimental boundary layer and of the repeatability of the measurements.

Results of a test of the linearity of the boundary-layer response with varying free-stream disturbance amplitudes are shown in figure 13. The disturbance amplitude,  $u'_{fs}$ , was always set at the edge of the boundary layer,  $\eta = 8$ , at a fixed streamwise location,  $R = 630$ . The boundary-layer response was found to be linear for forcing amplitudes

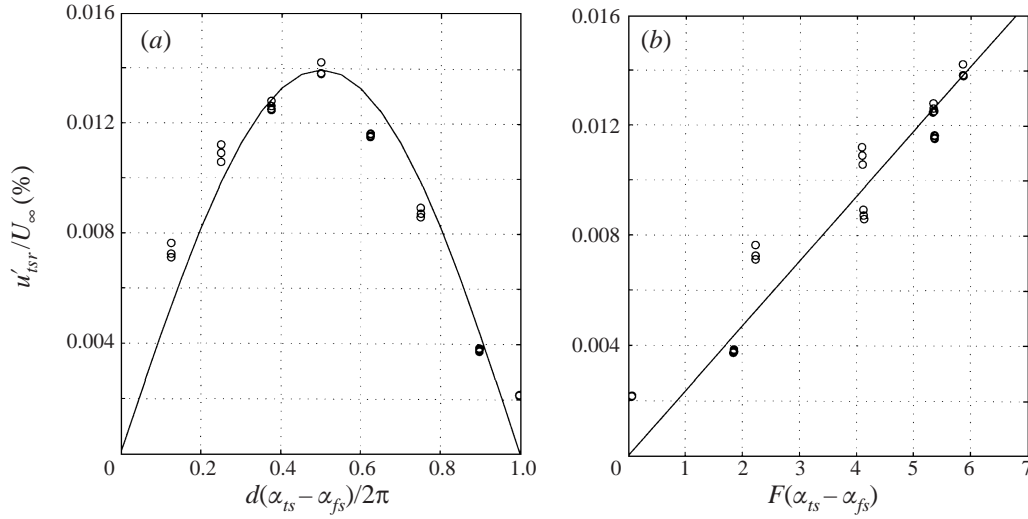


FIGURE 15. (a) TS amplitude variation with roughness width: measured data ( $\circ$ ),  $\sin(d(\alpha_{ts} - \alpha_{fs})/2)$  (—). (b) TS amplitude versus the Fourier transform of the roughness geometry evaluated at  $\alpha_{ts} - \alpha_{fs}$ : measured data ( $\circ$ ), linear variation (—).  $F = 50$ ,  $u'_{fs}/U_\infty = 0.3\%$ . Single roughness element, 100  $\mu\text{m}$  thick at  $R_r = 620$ .

up to 1% of the free-stream velocity. In figure 14 the results of a test of linearity with roughness height show that the response remained linear for non-dimensional roughness heights  $h = h^*/\delta_r$  of less than 0.2 ( $\delta_r = (vx/U_\infty)^{1/2}$ ), which corresponds to an asymptotically scaled roughness height  $h^*/(xe^5)$  of 1 ( $\epsilon = R^{-1/4}$ ). This result is similar to that found for acoustic receptivity by Saric *et al.* (1991), and by Zhou *et al.* (1994), and agrees with the acoustic receptivity calculations of Bodonyi (1990) who predicted a nonlinear response when the roughness exceeds the height of the viscous lower deck of triple-deck theory,  $h^*/(xe^5) > 1$ .

The final test of (1.1) was to verify that the boundary-layer response varied with the spatial Fourier transform of the surface geometry evaluated at a wavenumber equal to the difference between the wavenumber of the TS wave and the wavenumber of the free-stream disturbance. The forward transform is defined as

$$F(\alpha) = \int_{-\infty}^{\infty} H(x)e^{-i\alpha x} dx, \quad (3.2)$$

where  $H(x)$  describes the surface geometry. For a single rectangular roughness element of width  $d$  and height  $h$ , the transform, evaluated at  $(\alpha_{ts} - \alpha_{fs})$ , is given by

$$F(\alpha_{ts} - \alpha_{fs}) = \frac{2h}{\alpha_{ts} - \alpha_{fs}} \sin\left(\frac{d(\alpha_{ts} - \alpha_{fs})}{2}\right). \quad (3.3)$$

For constant  $\alpha_{ts}$  and  $\alpha_{fs}$  this function is maximum for a strip of width  $d = \pi/(\alpha_{ts} - \alpha_{fs})$  (half the wavelength corresponding to the resonant wavenumber  $\alpha_w = (\alpha_{ts} - \alpha_{fs})$ ). Measurements of the TS amplitude excited by roughness elements of various widths positioned at the branch I location are plotted in figure 15(a), where  $d$  has been normalized by the resonant wavelength  $2\pi/(\alpha_{ts} - \alpha_{fs})$ . The function  $\sin(d(\alpha_{ts} - \alpha_{fs})/2)$  is also included in the figure and a reasonable correlation between this function and the experimental data is apparent. Clearly, the generation of TS waves is tuned to the resonant wavenumber. In figure 15(b) the same data are used to illustrate the

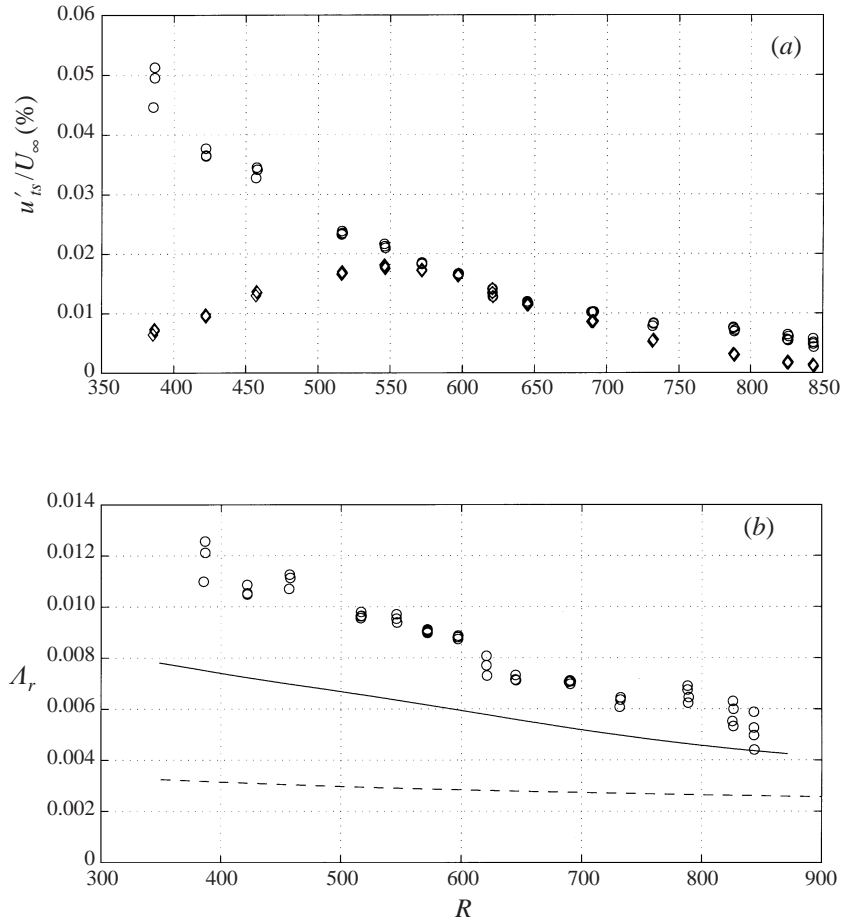


FIGURE 16. (a) TS amplitude variation with roughness Reynolds number:  $u'_{tsr}$ , downstream amplitudes extrapolated back to the roughness location ( $\circ$ );  $u'_{tsl}$ , downstream amplitudes extrapolated back to the branch I location ( $\diamond$ ). (b) Variation of the receptivity efficiency function with roughness Reynolds number: measurements ( $\circ$ ), finite Reynolds number calculations (—, Choudhari 1996), asymptotic theory (---, Kerschen 1991). Efficiency function is based on  $u'_{tsr}$ .  $F = 50$ ,  $u'_{fs}/U_\infty = 0.3\%$ . Single roughness element, 25.4 mm wide, 100  $\mu\text{m}$  thick.

linear variation of the boundary-layer response with the Fourier transform of the roughness geometry. The Fourier transform was evaluated using values of  $\alpha_{ts}$  from linear stability calculations.

These tests verified that the formulation of (1.1) was valid for free-stream forcing amplitudes less than 1% and for roughness heights less than  $0.2\delta_r$ . Within this linear regime, (1.1) was used to reduce the experimental data to an efficiency function. The dependence of this function on  $F$  and  $R_r$  is presented in the next section.

### 3.5. Receptivity at local roughness

The variation of local receptivity with roughness location was determined by repeating the measurement technique described in the previous section with a single roughness element positioned at a number of streamwise locations. The results, plotted in figure 16(a), show that the amplitude of the TS wave excited at the roughness decreases as the roughness is moved downstream. The effects of wave growth may

be included by using an effective branch I amplitude,  $u'_{tsI}$ , calculated by substituting the branch I Reynolds number,  $R_I$ , for the roughness Reynolds number,  $R_r$ , in the integration in (3.1). The effective branch I amplitudes are also plotted in figure 16(a). The large upstream amplitudes decay before reaching branch I and as a result, the effective branch I amplitude is maximum for a roughness location of  $R_r = 550$  which is just upstream of the branch I location,  $R_I = 613$ . This result is in agreement with results of the finite Reynolds number calculation of Crouch (1994a), who calculated a receptivity maximum well upstream of branch I but noted that when the growth of the eigenmode was included, the maximum moved back to a location just upstream of branch I. These experimental results also confirm the observation by a number of authors that roughness close to branch I will be the most critical in determining the downstream TS wave amplitudes.

Equations (1.1) and (3.3) were then used to determine values of the receptivity efficiency function from the TS amplitudes at each roughness location. This function, shown in figure 16(b), decreases with increasing roughness Reynolds number although the decay rate is not as great as that of the TS amplitudes in figure 16(a). This is primarily due to the magnitude of the Fourier transform of the roughness, which decreases as the TS wavenumber increases in the downstream direction. When the data are plotted in the form of the efficiency function, the effect of the Fourier transform is removed and the variation with roughness Reynolds number is reduced.

Results of calculations by Choudhari of the local receptivity of a Blasius boundary layer to a two-dimensional gust are included in figure 16(b). He reworked the calculations reported in Choudhari (1996) to match the experimental parameters. Disturbance profiles obtained from a numerical solution of the unsteady boundary layer equations (figure 8), were used as the input to his Orr–Sommerfeld-based finite Reynolds number receptivity calculation. The calculated efficiency function is 30% lower than the experimental result but both exhibit a similar trend with roughness Reynolds number. The asymptotic efficiency function calculated by Kerschen (1991) is also included in the figure. The data, taken from Kerschen's figure 1, were scaled by  $U_b'^2 \epsilon / (2\pi)^{1/2}$  where  $U_b' = 0.332$  is the slope of the mean flow close to the wall and  $\epsilon = R^{-1/4}$ . The agreement between theoretical and experimental results is reasonable considering the limitations of the theory and the extraordinary sensitivity of the Blasius boundary layer's stability characteristics. The comparison with theory is discussed further in the next section.

In figure 17, the results of a test investigating the variation of receptivity with forcing frequency are presented. For this test the roughness strip was fixed at  $R = 620$  while the frequency of the convected disturbance was varied. The TS amplitude excited at the roughness decreases with increasing frequency. During this test, branch I, which is dependent on the forcing frequency, moves forward from  $R = 700$  for  $F = 35$  to  $R = 490$  for  $F = 75$ . As a result of this movement,  $u'_{tsI}$  is a maximum at  $F = 45$  after which it decays at a faster rate than  $u'_{tsr}$ . Again most of the variation in the TS amplitude can be attributed to the decreasing magnitude of the Fourier transform as the relevant wavenumber ( $\alpha_{ts} - \alpha_{fs}$ ) increases with increasing frequency. When the data are plotted in the form of the efficiency function (figure 17b), there is only a slight decrease over the frequency range investigated.

### 3.6. Receptivity at distributed roughness

Measurements of the receptivity at distributed roughness were made by adding roughness elements to the plate surface, distributed evenly about branch I and spaced to give the resonant wavenumber. At this wavenumber the TS waves generated at each

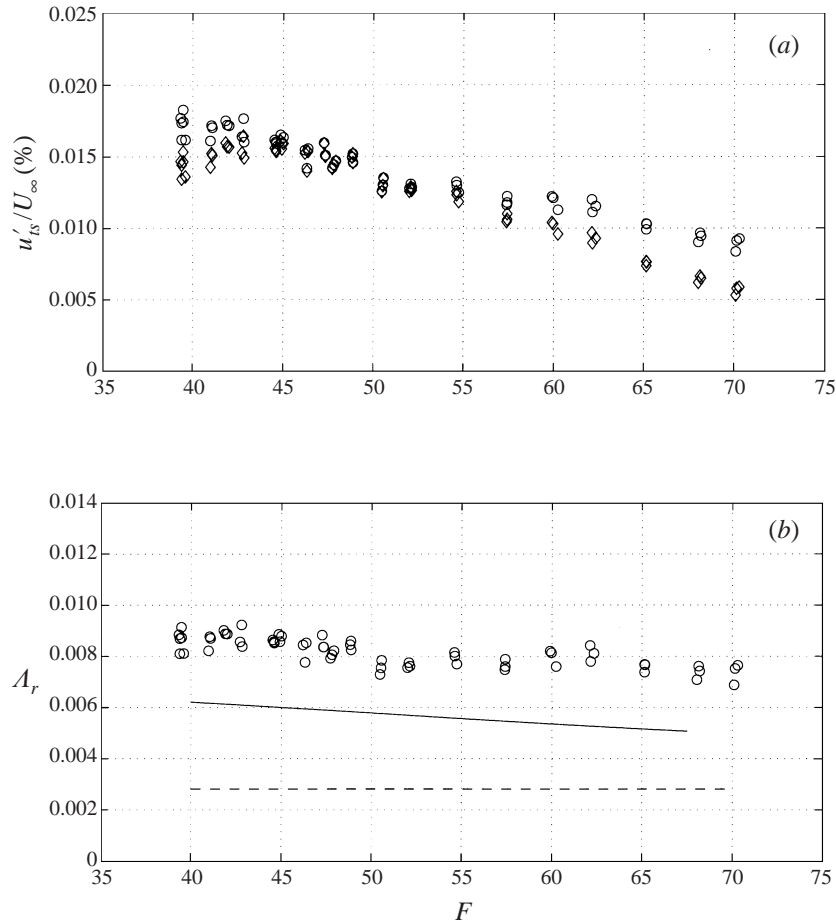


FIGURE 17. (a) TS amplitude variation with forcing frequency:  $u'_{tsr}$ , downstream amplitudes extrapolated back to the roughness location ( $\circ$ );  $u'_{tsl}$ , downstream amplitudes extrapolated back to branch I ( $\diamond$ ). (b) Variation of the receptivity efficiency function with frequency: measurements ( $\circ$ ), finite Reynolds number calculations (—, Choudhari 1996), asymptotic theory (- - -, Kerschen 1991). Efficiency function is based on  $u'_{tsr}$ .  $u'_{fs}/U_\infty = 0.3\%$ . Single roughness element, 25.4 mm wide, 100  $\mu\text{m}$  thick located at  $R = 620$ .

roughness element will add constructively. The increase in receptivity with increasing numbers of elements on the plate is shown in figure 18. The TS amplitude plotted here is calculated by assuming all wave generation occurs at branch I. The increase in receptivity is initially linear but starts to approach a limit with seven roughness elements on the plate. The increase is similar to that which would be obtained by summing the individual contributions of each roughness element. As the individual contributions decrease for roughness elements away from branch I, the receptivity to distributed roughness approaches an upper limit.

The variation in distributed receptivity with frequency is shown in figure 19. Unlike the single-roughness case shown earlier in figure 17(a), the effective branch I amplitudes for distributed roughness are highly tuned to the resonant frequency. This is due to interference between waves generated at successive roughness elements for TS wavenumbers away from the resonant wavenumber. The tuning effect may also be explained by considering the local geometry in the vicinity of branch I. As the

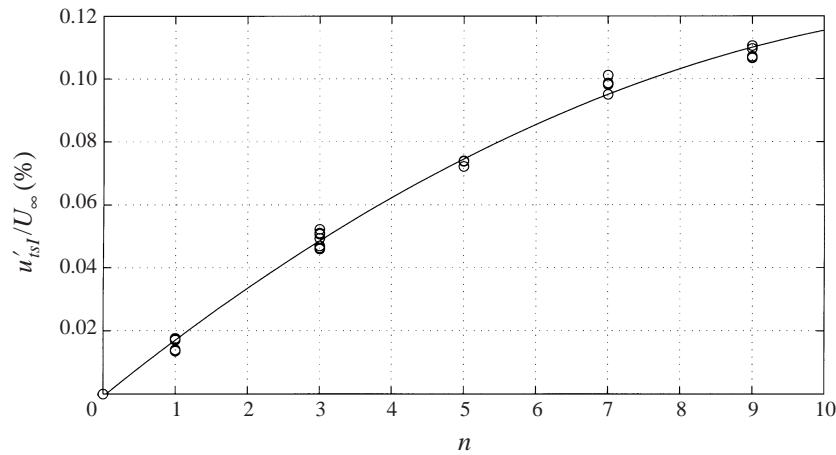


FIGURE 18. TS amplitude variation with number of roughness elements. Roughness elements 25.4 mm wide, 100  $\mu\text{m}$  thick, spaced 50.8 mm apart about  $R_l = 613$ .  $F = 50$ ,  $u'_{fs}/U_{\infty} = 0.3\%$ .

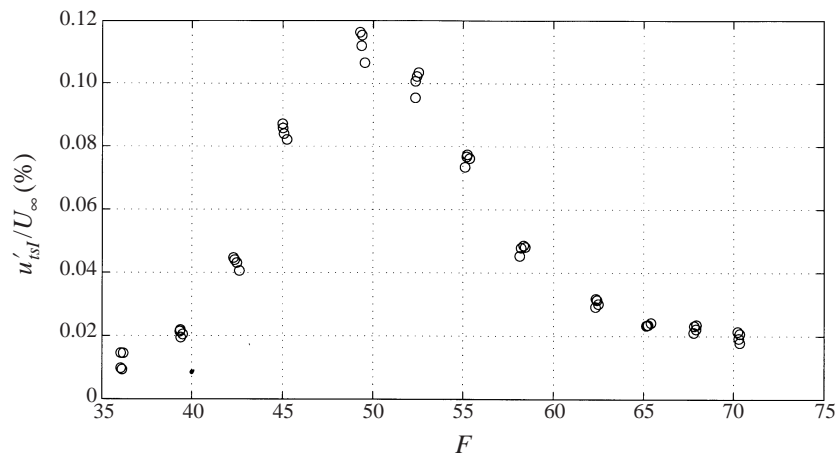


FIGURE 19. TS amplitude variation with forcing frequency. Downstream amplitude measurements extrapolated back to branch I. Array of nine roughness elements, 100  $\mu\text{m}$  thick, 25.4 mm wide, spaced 50.8 mm apart about  $R_l = 613$ .  $u'_{fs}/U_{\infty} = 0.3\%$ .

number of roughness elements is increased, the value of the Fourier transform at the resonant wall wavenumber,  $\alpha_{wall} = \pi/d = \alpha_{ts} - \alpha_{fs}$ , increases linearly and the peak in the transform at this wavenumber becomes increasingly narrow. The local analysis is only valid in the branch I region as the decay of waves forward of this region, and the reduced receptivity and reduced growth of waves aft of this region, reduces their contribution to the effective branch I amplitude. The results suggest that distributed receptivity could be calculated from the complex sum of a succession of local calculations. This approach was developed in detail by Choudhari & Streett (1994).

#### 4. Discussion and comparison with theory

A quantitative comparison of the experimental results with those of theory requires that the boundary-layer signature of the free-stream disturbance used in the

calculation matches that measured in the experiment (figure 8). The convected array of vortices introduced by Rogler & Reshotko (1975) and used by Crouch (1994*a, b*) and Lin *et al.* (1995) in their receptivity calculations has quite a different signature in the boundary layer than that measured in this experiment. The array of vortices produces a much higher fluctuation gradient close to the edge of the boundary layer (see Crouch 1994*b*, figure 2). As this is the region where the vortical receptivity mechanism is active, the results of the calculations are not comparable to the results of the experimental measurements reported here. In addition, Crouch's results are normalized by the vortex strength and so his efficiency function is dependent on the height of the vortex above the plate. The experimental efficiency function presented here is normalized by the fluctuation amplitude at the edge of the boundary layer and is independent of the wake height. Zavol'skii *et al.* (1983) and Choudhari (1994) assumed a Gaussian profile for the wake fluctuations. Such a profile does not fit the exponential scaling of the disturbance in the potential flow region outside the wake. As a result, the receptivity variation with wake height in these calculations is more extreme than that measured in this experiment. However, the convected gust disturbance calculated by Choudhari (1996) is similar to that measured in this experiment and a quantitative comparison between these calculations and the experimental results is possible.

The results of Choudhari's calculations were included in figures 16(*b*) and 17(*b*). The calculated efficiency function is 30% lower than the experimentally derived function but both exhibit the same trends with frequency and Reynolds number. The discrepancy between the theoretical and experimental results is considered to be small when the extreme sensitivity of the Blasius boundary layer's stability characteristics to the slightest pressure gradient is taken into account. As Blasius  $N$ -factors were used to estimate initial wave amplitudes from amplitudes measured downstream, any deviation from the Blasius profile would have had a large effect on the initial amplitude estimates. To illustrate this sensitivity, the experimental efficiency function was recalculated from the measured wave amplitudes, using stability results from a number of Falkner–Skan profiles. An exact match with the theory was obtained when  $N$ -factors for a Falkner–Skan profile with a  $\beta$  of  $-0.0075$  were used to reduce the data. This corresponds to flow past an expansion angle of  $0.02^\circ$ . The deviation of this profile from the Blasius profile is very small and the shape factor of 2.61 is only marginally higher than the Blasius value of 2.59. Such a profile is within the uncertainty of the experiment. This exercise demonstrates the extreme sensitivity of the experimental technique and shows that despite the care taken to establish a zero pressure gradient boundary layer, the uncertainty in the experimental efficiency function could be of the order of the discrepancy between the theoretical and experimental results.

The asymptotic efficiency function calculated by Kerschen (1991) was also included in figures 16(*b*) and 17(*b*). A rigorous comparison with the results of asymptotic theory would require that both the efficiency function and the Fourier transform be evaluated using first-order asymptotic results (Choudhari & Strett 1992). However, this would introduce an error in the transform, as the asymptotic estimate of the TS wavenumber significantly underestimates the experimentally validated Orr–Sommerfeld value. In addition, at first order the transform is evaluated at  $\alpha_{ts}$  instead of  $\alpha_{ts} - \alpha_{fs}$ . These errors are not included in the efficiency function comparisons reported here because the Fourier transform used in determining the experimental efficiency function was evaluated using TS wavenumbers from an Orr–Sommerfeld solution. Even so, the asymptotic estimate of the efficiency function is about 50% less than the finite Reynolds number estimate and has little variation with frequency or Reynolds number. The asymptotic scaling restricts the validity of the theory to the

branch I region at high Reynolds numbers and so the agreement would be expected to improve at higher Reynolds numbers.

The distributed receptivity results may be qualitatively compared with the results of calculations of Crouch (1994*a*). He calculated a factor of 10 increase in the receptivity at a wavy wall compared with that at local roughness near branch I. He also calculated the increased tuning of TS wave amplitudes about the resonant wall wavenumber. His results agree with the order of magnitude increase in receptivity measured in this experiment and the resonant response of the boundary layer over distributed roughness. As the form of his convected disturbance differed from that measured in the experiment, a quantitative comparison with his calculations is not possible.

A comparison may also be made with experimental and theoretical results for acoustic receptivity. The value of the efficiency function calculated by Crouch (1992) for acoustic receptivity at local roughness with a forcing frequency  $F = 56$  and with the roughness at branch I was 0.06. A similar value was obtained by Choudhari & Streett (1992) whose calculations matched the experimental results of Wiegel & Wlezien (1993). This value is 10 times the convected receptivity measured in this experiment. Crouch (1994*a*) calculated acoustic receptivity to be 20 times stronger than vortical receptivity, but as his vortical receptivity is referenced to the strength of the vortex, the results are dependent on the height of the vortex above the wall. Choudhari (1994) estimated the acoustic receptivity to be 100 times stronger than the receptivity to a compact Gaussian wake, but again the use of the wake amplitude as the reference makes the results dependent on the height of the wake above the wall. An acoustic disturbance is not localized in the free stream and so the location of the reference amplitude is not critical. However, for localized vortical disturbances, the location of the reference amplitude directly affects the receptivity value. Therefore, for a valid comparison between acoustic disturbances and localized vortical disturbances, the amplitude of the streamwise velocity fluctuations at the edge of the boundary layer should be used as the reference amplitude for both disturbances. This choice makes the vortical efficiency function independent of the height of the disturbance above the surface. With this choice of reference, local acoustic receptivity is 10 times greater than local vortical receptivity. Although the receptivity mechanism for acoustic disturbances is stronger than the mechanism for convected disturbances, the relative importance of each mechanism to a particular flow will depend on the relative strength of the acoustic or vortical disturbances in the free stream. It should be noted that although a two-dimensional harmonic acoustic disturbance is a reasonable representation of free-stream sound, a two-dimensional harmonic convected disturbance is a very simplified model of the vorticity in free-stream turbulence. Hence, the implications of these results to more complicated flow fields must be qualified by the applicability of the convected-vorticity model.

## 5. Conclusions

Evidence which tends to validate the linear theory describing the local receptivity of a boundary layer to convected disturbances at surface roughness has been obtained in a series of experiments on a flat-plate Blasius boundary layer. The wake from a vibrating ribbon, positioned well upstream of the plate leading edge, provided an effective convected disturbance for forcing the boundary layer. It was shown that this free-stream disturbance could be defined in terms of the streamwise fluctuations at the edge of the boundary layer, removing the need for a wake-height parameter in the



receptivity analysis. The response of the boundary layer to the convected disturbance was confined to the outer portion of the layer with streamwise fluctuations being rapidly damped towards the wall. However, the outer-layer interaction between the convected disturbance and the short-scale mean-flow distortion due to the roughness was sufficient to excite measurable TS waves. It was demonstrated that receptivity to convected disturbances was the dominant mechanism responsible for the generation of these waves and that the measured mode shape, growth rate and phase speed of the waves matched that of TS waves predicted by linear stability theory.

Tests were performed to determine the range of validity of linear assumptions made in current receptivity theories. Linear variation with forcing amplitude was demonstrated for boundary-layer edge amplitudes up to 1% of the free-stream velocity. The TS amplitude was also shown to vary linearly with roughness height until the roughness exceeded  $0.2\delta_r$ . Finally, the influence of roughness geometry was shown to be well modelled by the spatial Fourier transform of the roughness evaluated at a wavenumber equal to the difference between the wavenumber of the TS wave and the wavenumber of the free-stream disturbance. Variations in the value of this transform due to variations in either of these two wavenumbers explained much of the variation observed in the measured TS amplitudes.

The receptivity results were then expressed in the form of an efficiency function,  $A(F, R)$ , which is independent of the effects of the free-stream disturbance amplitude, the roughness height and the roughness geometry. This function was shown to decrease monotonically with  $F$  and  $R$ , although the variation was slight over the ranges investigated. The experimental results were compared with results of the Orr–Sommerfeld-based finite Reynolds number receptivity calculations of Choudhari (1996) and with results of the asymptotic theory of Kerschen (1991). Better agreement was obtained with the finite Reynolds number results as would be expected since the asymptotic scalings are only valid at large Reynolds numbers. The finite Reynolds number results were approximately 30% lower than the experimental data but showed equivalent trends with frequency and Reynolds number. The agreement between theory and experiment is reasonable considering the limitations of the theory and the extreme sensitivity of the stability characteristics of the Blasius boundary layer to the slightest pressure gradient.

The measured TS amplitudes with distributed roughness on the plate were highly tuned to the resonant frequency where the TS wavenumber was equal to the sum of the free stream and wall wavenumbers. This result, plus the linear increase in TS amplitude with increasing number of roughness elements, can be explained in terms of the Fourier transform of the distributed roughness which exhibits the same characteristics. The data agree qualitatively with results of finite Reynolds number calculations by Crouch (1992) of the receptivity of a boundary layer over a wavy wall. As the form of his convected disturbance differed from that measured in this experiment, a quantitative comparison with his calculations was not possible. The data also support the observation by Choudhari & Streett (1994) that the total distributed receptivity could be calculated from the complex sum of a succession of local calculations.

A comparison with previous acoustic receptivity results indicates that the vortical receptivity efficiency function based on the streamwise forcing at the boundary-layer edge is a factor of 10 less than the acoustic receptivity efficiency function. The choice of the amplitude at the edge of the boundary layer as the disturbance amplitude makes this factor somewhat smaller than that reported by previous investigators. Although the acoustic receptivity mechanism is stronger, the relative importance of

each mechanism in a particular flow will be dependent on the composition of the free-stream disturbance field. This comparison should be qualified by the fact that although the acoustic receptivity function is based on an accurate model of free-stream sound, the vortical receptivity function is based on a simplified model of free-stream turbulence.

The measurements reported here have validated many aspects of the theory for receptivity to single-frequency two-dimensional convected disturbances at two-dimensional roughness. The work has been extended to broad-band two-dimensional convected disturbances by Dietz (1998). It is a step towards determining the receptivity to free-stream turbulence with its broad-band three-dimensional spectrum.

The experiment was aided by the work and advice of Dr M. Choudhari who also provided the finite Reynolds number results reported in the paper. The advice and support of Dr S. Davis is also gratefully acknowledged. In addition, thanks are due to Dr M. Malik for the use of his stability code and to Professor E. Kerschen and Dr J. Crouch for several fruitful discussions. This work was performed while the author held a National Research Council–Ames Research Associateship.

#### REFERENCES

- AIZIN, L. B. & POLYAKOV, N. F. 1979 Acoustic generation of Tollmien–Schlichting waves over local unevenness of surfaces immersed in streams. *Preprint 17, Akad. Nauk USSR, Siberian Div., Inst. Theor. Appl. Mech., Novosibirsk* (in Russian).
- BODONYI, R. J., WELCH, W. J. C., DUCK, P. W. & TADJIFAR, M. 1989 A numerical study of the interaction between unsteady free-stream disturbances and localized variations in surface geometry. *J. Fluid Mech.* **209**, 285–308.
- BREUER, K. S., DZENITIS, G., GUNNARSSON, J. & ULLMAR, M. 1996 Linear and nonlinear evolution of boundary layer instabilities generated by acoustic-receptivity mechanisms. *Phys. Fluids* **8**, 1415–1423.
- CHOU DHARI, M. 1994 Localized and distributed boundary-layer receptivity to convected unsteady wake in free stream. *NASA CR-4578*.
- CHOU DHARI, M. 1996 Boundary-layer receptivity to three-dimensional unsteady vortical disturbances in free stream. *AIAA Paper* 96-0181.
- CHOU DHARI, M. & STREETT, C. L. 1992 A finite Reynolds number approach for the prediction of boundary-layer receptivity in localized regions. *Phys. Fluids A* **4**, 2495–2514.
- CHOU DHARI, M. & STREETT, C. L. 1994 Theoretical prediction of boundary-layer receptivity. *AIAA Paper* 94-2223.
- CROUCH, J. D. 1992 Localized receptivity of boundary layers. *Phys. Fluids A* **4**, 1408–1414.
- CROUCH, J. D. 1994a Theoretical studies on the receptivity of boundary layers. *AIAA Paper* 94-2224.
- CROUCH, J. D. 1994b Distributed excitation of Tollmien–Schlichting waves by vortical free-stream disturbances. *Phys. Fluids* **6**, 217–223.
- CROUCH, J. D. & BER TOLOTTI, F. P. 1992 Nonlocalized receptivity of boundary layers to three-dimensional disturbances. *AIAA Paper* 92-0740.
- CROUCH, J. D. & SPALART, P. R. 1995 A study of non-parallel and nonlinear effects on the localized receptivity of boundary layers. *J. Fluid Mech.* **290**, 29–37.
- DAVIS, S. S. 1997 Wave excitation in an unsteady boundary layer. *AIAA Paper* 97-1833.
- DIETZ, A. J. 1996 Distributed boundary layer receptivity to convected vorticity. *AIAA Paper* 96-2083.
- DIETZ, A. J. 1998 Boundary-layer receptivity to transient convected disturbances. *AIAA J.* **36**, 1171–1177.
- GASTER, M. 1965 On the generation of spatially growing waves in a boundary layer. *J. Fluid Mech.* **22**, 433–441.
- GOLDSTEIN, M. E. 1983 The evolution of Tollmien–Schlichting waves near a leading edge. *J. Fluid Mech.* **127**, 59–81.

- GOLDSTEIN, M. E. 1985 Scattering of acoustic waves into Tollmien–Schlichting waves by small streamwise variations in surface geometry. *J. Fluid Mech.* **154**, 509–29.
- GOLDSTEIN, M. E. & HULTGREN, L. S. 1987 A note on the generation of Tollmien–Schlichting waves by sudden surface-curvature change. *J. Fluid Mech.* **181**, 519–525.
- GOLDSTEIN, M. E., SOCKOL, P. M. & SANZ, J. 1983 The evolution of Tollmien–Schlichting waves near a leading edge. Part 2. Numerical determination of amplitudes. *J. Fluid Mech.* **129**, 443–453.
- HILL, D. C. 1995 Adjoint systems and their role in the receptivity problem for boundary layers. *J. Fluid Mech.* **292**, 183–204.
- KACHANOV, Y. S., KOZLOV, V. V. & LEVCHENKO, V. YA. 1978 Occurrence of Tollmien–Schlichting waves in the boundary layer under the effect of external perturbations. *Izv. Akad. Nauk SSSR Mekh. Zhid. i Gaza* **5**, 85–94 (in Russian). (Transl. *Fluid. Dyn.* **13**, 1979, 704–711).
- KERSCHEN, E. 1989 Boundary layer receptivity. *AIAA Paper* 89-1109.
- KERSCHEN, E. J. 1990 Boundary layer receptivity theory. *Appl. Mech. Rev.* **43**, S152–S157.
- KERSCHEN, E. J. 1991 Linear and non-linear receptivity to vortical free-stream disturbances. In *Boundary Layer Stability and Transition to Turbulence* (ed. D. C. Reda, H. L. Reed & R. K. Kobayashi). ASME FED, vol. 114, pp. 43–48.
- LEEHEY, P. & SHAPIRO, P. 1979 Leading edge effect in laminar boundary layer excitation by sound. *Laminar-Turbulent Transition* (ed. R. Eppler & H. Fasel), pp. 321–331. Springer.
- LIN, N., STUCKERT, G. K. & HERBERT, TH. 1995 Boundary layer receptivity to freestream vortical disturbances. *AIAA Paper* 95-0772.
- MALIK, M. R. 1989  $e^{Malik}$  a new spatial stability analysis program for transition prediction using the  $e^N$  method. *High Technology Rep.* HTC-8902.
- MURDOCK, J. W. 1980 The generation of a Tollmien–Schlichting wave by a sound wave. *Proc. R. Soc. Lond. A* **372**, 517–534.
- NISHIOKA, M. & MORKOVIN, M. V. 1986 Boundary-layer receptivity to unsteady pressure gradients: experiments and overview. *J. Fluid Mech.* **171**, 219–261.
- PAREKH, D., PULVIN, P. & WLEZIEN, R. W. 1991 Boundary layer receptivity to convected gusts and sound. In *Boundary Layer Stability and Transition to Turbulence* (ed. D. C. Reda, H. L. Reed, & R. K. Kobayashi). ASME FED, vol. 114, pp. 69–75.
- RESHOTKO, E. 1976 Boundary-layer stability and transition. *Ann. Rev. Fluid Mech.* **8**, 311–349.
- ROGLER, H. L. & RESHOTKO, E. 1975 Disturbances in a boundary layer introduced by a low intensity array of vortices. *SIAM J. Appl. Maths* **28**, 431–462.
- RUBAN, A. I. 1985 On the generation of Tollmien–Schlichting waves by sound. *Fluid Dyn.* **19**, 709–716.
- SARIC, W. S. 1990 Low-speed experiments: Requirements for stability measurements. In *Instability and Transition 1* (ed. M. Y. Hussaini & R. G. Voigt), pp. 162–174. Springer.
- SARIC, W. S., HOOS, J. A. & RADEZTSKY, R. H. 1991 Boundary-layer receptivity of sound with roughness. In *Boundary Layer Stability and Transition to Turbulence* (ed. D. C. Reda, H. L. Reed, & R. K. Kobayashi), ASME FED, vol. **114**, pp. 17–22.
- SCHUBAUER, G. B. & SKRAMSTAD, H. K. 1948 Laminar-boundary-layer oscillations and transition on a flat plate. *NACA TR*-909.
- WIEGEL, M. & WLEZIEN, R. 1993 Acoustic receptivity of laminar boundary layers over wavy walls. *AIAA Paper* 93-3280.
- WLEZIEN, R. W., PAREKH, D. E. & ISLAND, T. C. 1990 Measurement of acoustic receptivity at leading edges and porous strips. *Appl. Mech. Rev.* **43**, S167–S174.
- WYGNANSKI, I., CHAMPAGNE, F. & MARASLI, B. 1986 On the large-scale structures in two-dimensional, small-deficit, turbulent wakes. *J. Fluid Mech.* **168**, 31–71.
- ZAVOL'SKII, N. A., REUTOV, V. P. & RYBUSHKINA, G. V. 1983 Generation of Tollmien–Schlichting waves via scattering of acoustic and vortex perturbations in boundary layer on a wavy surface. *J. Appl. Mech. Tech. Phys.* **24**, 355–361.
- ZHOU, M. D., LIU, D. P. & BLACKWELDER, R. F. 1994 An experimental study of receptivity of acoustic waves in laminar boundary layers. *Exps. Fluids* **17**, 1–9.